

# Spin-orbit interaction and molecular-field effects in the $L_{2,3}VV$ Auger-electron spectra of HCl

Reinhold F. Fink

*Theoretische Chemie, Ruhr-Universität Bochum, D-44780 Bochum, Germany*

Mika Kivilompolo, Helena Aksela, and Seppo Aksela

*Department of Physical Sciences, University of Oulu, FIN-90570 Oulu, Finland*

(Received 27 February 1998)

*Ab initio* calculations based on quantum chemical methods and the one center approximation have been carried out for the  $L_{2,3}VV$  normal Auger-electron spectrum of HCl. Spin-orbit and molecular field effects were explicitly included in the description of the intermediate  $2p$  core hole state. The results are compared with the experimental spectrum obtained with synchrotron radiation. The corresponding atomic  $L_{2,3}MM$  Auger transitions are studied in the isoelectronic argon atom. The calculated Auger electron spectra are in good agreement with the experimental and to previous theoretical results. For HCl the calculations predict substantially different total Auger transition probabilities of 126, 99, and 113 meV for the three nondegenerate spin-orbit and molecular-field-split  $2p^{-1}$  states:  $2p_{3/2}^{-1}(^2\Pi_{3/2})$ ,  $2p_{3/2}^{-1}(^2\Sigma^+_{1/2})$ , and  $2p_{1/2}^{-1}(^2\Pi_{1/2})$ , respectively. Furthermore, each of these core hole states gives rise to remarkably different intensity distributions. These effects are explained by (i) the partial orientation of the chlorine  $2p$  core hole by the molecular field, (ii) a decrease of the net population of the chlorine  $3p$  orbital in the bond direction due to the chemical bond, and (iii) the clear (97%) preference of the Auger decay of an oriented  $2p$  core orbital to produce final states with at least one hole in the  $3p$  orbital with the same spatial orientation. [S1050-2947(98)00609-X]

PACS number(s): 33.80.-b, 32.80.Hd, 82.80.Pv

## I. INTRODUCTION

Auger-electron spectra, especially of molecules and condensed matter, contain many structures overlapping heavily with each other. This is due to the large number of energetically nearly spaced electronic and vibrational states both in the intermediate and final state of the process. From experiments it is usually impossible to reliably separate the different contributions. A possible way out is to produce a theoretical counterpart, a theoretical spectrum, and to compare it with the experimental one. If the profiles are in good resemblance to each other, then a deeper understanding of the physics involved becomes possible. The demands for the theory are high; the theoretical calculations should account for all the essential things affecting in the course of the transitions to be able to reproduce the experiment. In this article we describe a method that is designed to be routinely applicable for an accurate calculation of fully theoretical  $L_{2,3}VV$  Auger electron spectra of molecules.

So far, almost all theoretical studies of molecular Auger electron spectra have been done for the  $KVV$  type of transitions (see, e.g., [1–3], and references therein). Only relatively few studies exist for intermediate core holes with higher  $l$  values. Probably the most sophisticated work in this field is the calculation of the  $L_{2,3}VV$  Auger-electron spectrum of HCl by Kvalheim [4]. He used Auger transition amplitudes of the argon atom and a configuration interaction (CI) method for the description of the final states. More recently, Chelkowska and Larkins [5] described the calculation of molecular Auger electron spectra on the basis of the “one center approximation” [6] in the cases when  $s$ -,  $p$ -, and  $d$ -type atomic orbitals are involved in the Auger process as core hole or valence orbitals. As an example, they calculated the  $L_{2,3}VV$  Auger electron spectrum of HCl. But, as the aim

of the paper was not a detailed reproduction of the Auger-electron spectrum, hence, their results compare less favorably to the experimental spectrum. The  $L_{2,3}VV$  Auger-electron spectrum of HCl was also calculated by Sukhorukov *et al.* [7,8] with a partially semiempirical approach. These authors also considered  $L_{2,3}V-VVV$  shake satellite decay and its influence on the Auger electron spectrum [8].

Using the semiempirical intermediate neglect of differential overlap (INDO) approach, Larkins and co-workers calculated the  $L_{2,3}VV$  Auger electron spectra of  $\text{SiH}_4$  [9] and several phosphorus compounds [10]. Furthermore, the Auger-electron spectrum of  $\text{SiF}_4$  has been calculated recently by Cederbaum and Tarantelli and interpreted with the foreign imaging scheme [11]. In that work the intensities of the Auger transitions were estimated by the two-hole population analysis [12]. Finally, there exist some theoretical treatments of solid-state Auger electron spectra [13] in which the transition matrix elements were obtained from atomic codes and some additional assumptions for the crystal-field splittings and spectral broadenings were included.

All approaches discussed so far did not explicitly account for the molecular field, which is known to contribute to the splitting of  $l \neq 0$  core-hole states besides the dominating spin-orbit effect. Pioneering experimental studies of the ligand field splitting have been done by Bancroft and co-workers (see, e.g., Ref. [14] and references therein). Recently it became possible to resolve the molecular-field splitting of  $2p$  core-hole states in experimental photo electron spectra of several sulfur compounds [15–17] and of HCl [18]. Insight in the structure of the molecular-field split core-hole states has been provided by several theoretical investigations: Gel'mukhanov *et al.* [17] and Børve *et al.* [15,19] demonstrated that these splittings can be reproduced and understood by the nonrelativistic energies of the core-hole states,

that can be obtained from *ab initio* calculations, and an effective Hamiltonian that accounts for the spin-orbit interaction in the  $2p$  orbitals. Very recently, Ellingsen *et al.* [20] presented a higher level approach by a fully relativistic CI calculation of the  $2p^{-1}$  states of HCl.

Using the  $\text{H}_2\text{S } L_{2,3}VV$  Auger decay as an example Gel'mukhanov *et al.* [17] showed that the three  $2p^{-1}$  states have substantially different partial Auger decay rates into the lowest  $2b_1^{-2}(^1A_1)$  final state. Comparable effects were found experimentally in the Auger electron spectra of HCl [18] and of the HS radical [21]. In the last three articles it was demonstrated that the three core-hole states give rise to very different intensity distributions in the Auger-electron spectrum. This was interpreted qualitatively for the decay in some final states. But, to our knowledge, calculations of (i) fully theoretical  $L_{2,3}$  Auger electron spectra of molecules and (ii) complete Auger electron spectra of the different  $2p$  core-hole states were not done so far.

In this paper we will, therefore, describe a theoretical method that is able to provide this. It is based on *ab initio* CI calculations with nonrelativistic molecular programs that are driven by a Gaussian basis set, the ‘‘one center approximation,’’ [6] and reasonable estimates for the line forms. We demonstrate the suitability of this method at the  $L_{2,3}VV$  Auger-electron spectrum of HCl and the  $L_{2,3}MM$  Auger-electron spectrum of argon, which are both compared to recent experimental data.

The article is subdivided as follows: Experimental details are briefly described in Sec. II. This is followed by a description of the theory and the numerical methods in Sec. III. We present, compare, and discuss our theoretical and experimental  $L_{2,3}MM$  Auger-electron spectra of argon in Sec. IV. Section V gives our results for the  $2p$  core-hole states of HCl that are used for Sec. VI which includes our results for the corresponding  $L_{2,3}VV$  Auger-electron spectrum. In Sec. VII we explain the remarkable dependence of the predicted total and partial transition rates of different molecular field and spin-orbit split core-hole states. In Sec. VIII we sum up how an accurate calculation of  $L_{2,3}VV$  Auger transitions should be done and give our conclusions.

## II. EXPERIMENT

The synchrotron radiation excited electron spectra have been measured at the ‘‘Finnish beam line’’ bl 51 [22] of the MAX-I storage ring in Lund, Sweden. Synchrotron radiation is obtained from a short period undulator [23]. The useful photon energy range for gas phase electron spectroscopy at the bl 51 is 60–300 eV. The radiation is monochromatized by the modified SX-700 plane grating monochromator [24]. The important part for the gas phase experiments is the differential pumping stage that reduces the pressure five orders of magnitude between the experimental chamber and the high vacuum monochromator. It also contains a toroidal refocusing mirror in order to create a minimal spot size at the source point of the electron spectrometer. The used electron spectrometers were equipped with hemispherical analyzers either at a fixed angle (SES-144) [25] or at variable angle (SCIENTA-200) [26] with respect to the horizontal polarization direction of the synchrotron radiation. Both analyzers apply retarding lenses and position-sensitive detector sys-

tems that are very crucial for intensity reasons when working at low-energy second generation storage rings. The energy resolution of the SES-144 analyzer was about 65 meV using a typical pass energy of 20 eV.

The  $L_{2,3}VV$  Auger-electron spectrum of HCl was obtained with the photon energy of 254 eV, which is still well below the chlorine  $L_1$  edge at 278.3 eV [27] in order to avoid cascade Auger transitions. Note that in previously reported electron-impact excited Auger-electron spectra [28,29] such cascade Auger decay of the  $L_1$  core hole was possible. As recently demonstrated for argon [30], the contribution of such effects to Auger-electron spectra can be remarkably large. We should mention that the photon energy used in this experiment is sufficient to reach several shakeup and shake-off states of the core-ionized HCl molecule. According to the work of Carravetta *et al.* [31] the highest intensities for these transitions are between 12 and 25 eV above the  $2p_{3/2}$  ionization threshold (207.3 eV [27]).

For argon, we discuss here the recently reported measurements by Pulkkinen *et al.* [32]. The photon energy of 265 eV in the experiment was below the first  $2p^{-1}3s^23p^54p^1$  shakeup resonance (270.9 eV [33]) but still well above the  $2p$  ionization edges (248.63 and 250.78 eV [34] of  $2p_{3/2}$  and  $2p_{1/2}$ , respectively).

In these experiments postcollision interaction (PCI) effects influence the energetical positions and shapes of the Auger lines but should not be a dominating effect. Thus, we did not account for PCI effects in the theoretical spectra but we shifted the experimental spectra to the nominal Auger energies. The kinetic energy of the argon spectrum was adjusted to the  $L_3M_{2,3}M_{2,3}(^1D_2)$  line at 203.499-eV kinetic energy [32]. The spectrum of HCl was adjusted to the  $2p_{1/2}^{-1} \rightarrow 2\pi^{-2}(^3\Sigma^-)$  line at 173.35-eV kinetic energy or 35.68 eV binding energy [29].

## III. THEORY AND NUMERICAL METHODS

### A. Spin-orbit interaction for $2p$ core holes

A description of the spin-orbit interaction and molecular-field effects on the energy levels of the core-ionized states and on the intensity patterns of molecular  $L_{2,3}VV$  Auger-electron spectra was recently given by Gel'mukhanov *et al.* [17]. A detailed investigation of the nature of the spin-orbit and molecular-field-split core ionized states and a method for calculation can be found in the work of Børve and co-workers [15,19]. However, we shall briefly present our approach to this problem, which uses the Cartesian orbitals  $2p_x$ ,  $2p_y$ , and  $2p_z$ . The spin-orbit operator

$$\hat{H}_{\text{SO}} = -\gamma \cdot \vec{s} \cdot \vec{l}, \quad (1)$$

where  $\gamma$  is the spin-orbit parameter, is constructed in the basis  $((2p_x\alpha)^{-1}, i(2p_y\alpha)^{-1}, -(2p_z\beta)^{-1})$  and  $((2p_x\beta)^{-1}, -i(2p_y\beta)^{-1}, (2p_z\alpha)^{-1})$ , yielding, in both basis sets, the same matrix representation

$$\mathbf{H}_{\text{SO}} = -\frac{\gamma}{2} \begin{pmatrix} 0 & 1 & 1 \\ 1 & 0 & 1 \\ 1 & 1 & 0 \end{pmatrix}. \quad (2)$$

TABLE I. Eigenvalues and eigenvectors of the atomic spin-orbit operator [Eq. (2)], core hole densities of the  $2p_x$ ,  $2p_y$ , and  $2p_z$  orbitals ( $\mathcal{D}_x, \mathcal{D}_y, \mathcal{D}_z$ ) and the  $LS$  term used for linear molecules.

$J$	$M_J$	Eigenvalue	Eigenvector	$\mathcal{D}_x$	$\mathcal{D}_y$	$\mathcal{D}_z$	$LS$ term
$\frac{3}{2}$	$\frac{3}{2}$	$-\gamma/2$	$\left(\frac{1}{\sqrt{2}}, -\frac{1}{\sqrt{2}}, 0\right)$	$\frac{1}{2}$	$\frac{1}{2}$	0	${}^2\Pi_{3/2}$
$\frac{3}{2}$	$\frac{1}{2}$	$-\gamma/2$	$\left(\frac{1}{\sqrt{6}}, \frac{1}{\sqrt{6}}, -\sqrt{\frac{2}{3}}\right)$	$\frac{1}{6}$	$\frac{1}{6}$	$\frac{2}{3}$	${}^2\Sigma_{1/2}^+$
$\frac{1}{2}$	$\frac{1}{2}$	$\gamma$	$\left(\frac{1}{\sqrt{3}}, \frac{1}{\sqrt{3}}, \frac{1}{\sqrt{3}}\right)$	$\frac{1}{3}$	$\frac{1}{3}$	$\frac{1}{3}$	${}^2\Pi_{1/2}$

The two basis sets represent the two degenerate Kramers doublets of the spin-orbit split configurations.

The advantage of representing the core hole in this Cartesian basis is the simple form of the spin-orbit operator in this representation, as the coordinate system can be chosen for any molecule in such a form that the molecular field effects appear only on the diagonal elements of the total Hamiltonian ( $H_{\text{core}}$ ):

$$\mathbf{H}_{\text{core}} = \begin{pmatrix} \epsilon_x & -\frac{\gamma}{2} & -\frac{\gamma}{2} \\ -\frac{\gamma}{2} & \epsilon_y & -\frac{\gamma}{2} \\ -\frac{\gamma}{2} & -\frac{\gamma}{2} & \epsilon_z \end{pmatrix}. \quad (3)$$

$\epsilon_x$ ,  $\epsilon_y$ , and  $\epsilon_z$  are the nonrelativistic energies of the  $2p_x^{-1}$ ,  $2p_y^{-1}$ , and  $2p_z^{-1}$  states and include the molecular-field effects. Diagonalization of the matrix (3) leads to eigenvalues that are the spin-orbit and molecular-field-split energies of the  $2p^{-1}$  states.

The eigenvectors and eigenvalues of the spin-orbit matrix of an atom ( $\epsilon_x = \epsilon_y = \epsilon_z$ ) are collected in Table I. This table also includes the  $2p$  core-hole densities ( $\mathcal{D}$ ), which are obtained by squaring the coefficients of the corresponding eigenvectors. As we discuss below, these  $\mathcal{D}$  are of particular importance for the Auger transition rates. Note that for atoms the energy levels of the  $J = \frac{3}{2}$  and  $J = \frac{1}{2}$  states contain on average one-third of a hole in each of the  $2p$  orbitals.

In molecules the existence of the nonspherically symmetric molecular field causes a splitting of the  $J = \frac{3}{2}$  components of the core-hole states in two Kramers doublets. The wave functions of the core-ionized states of molecules are essentially the atomic wave functions in Table I. In this paper we will designate the HCl  $2p^{-1}$  states with the  $LS$  ( ${}^{(2S+1)}\Lambda_{M_J}$ ) terms  ${}^2\Pi_{3/2}$ ,  ${}^2\Sigma_{1/2}^+$ , and  ${}^2\Pi_{1/2}$ , which are also given in Table I. Of course, neither  $S$  nor  $\Lambda$  is good a quantum number for the current case of strong spin-orbit interaction, but the  $LS$  symbols correctly represent the dominating electronic configuration of the states.

## B. Auger transition probabilities

The determination of the Auger transition rates is in line with our previous work [3,35] and similar to the formulation of Chelkowska and Larkins [5]. We repeat the main ideas here for the current case of oriented  $2p^{-1}$  intermediate states.

We assume that the Auger process can be treated as a two-step process, which is a very good approximation for the present case. Then the partial Auger transition rate for the decay of the  $i$ th intermediate state to the  $f$ th final state becomes

$$\Gamma_{if} = 2\pi \sum_{lm} |\langle \Psi_i | \hat{H} - E | \mathcal{A} \Psi_f \varphi_c^{lm} \rangle|^2 \quad (4)$$

with  $\Psi_i$  and  $\Psi_f$  being the  $N-1$  and  $N-2$  electron wave functions of the intermediate state and final state, respectively ( $N$  is the number of electrons in the ground state).  $\mathcal{A}$  is the antisymmetrization operator,  $\varphi_c^{lm}$  is the continuum wave function representing the Auger electron in the channel  $lm$ .  $\hat{H}$  is the Hamiltonian of the system and  $E$  the energy of  $\Psi_i$ . In this work we describe the intermediate state exclusively by  $2p^{-1}$  configurations whereas the  $\Psi_f$ 's are represented by CI wave functions.

As discussed above the spin-orbit coupling causes the core-hole wave functions to be linear combinations of the Cartesian basis configurations of the preceding section, which we write here as  $\Psi_x$ ,  $\Psi_y$ , and  $\Psi_z$ , respectively. Equation (4) can now be written as

$$\Gamma_{if} = 2\pi \sum_{lm} \left| \sum_{\alpha}^{x,y,z} C_{i,\alpha} \langle \Psi_{\alpha} | \hat{H} - E | \mathcal{A} \Psi_f \varphi_c^{lm} \rangle \right|^2. \quad (5)$$

In our calculations we shall not consider the generally small effect of spin-orbit interaction in the final states. Therefore, the final-state wave function, including the continuum wave function, can be chosen without loss of generality as a purely real function and an eigenfunction of  $\hat{S}_z$ . As mentioned above, the  $\Psi_x$  and  $\Psi_z$  configurations have different magnetic quantum numbers ( $m_s$ ) and the coefficient of  $\Psi_y$  is purely imaginary whereas those of  $\Psi_x$  and  $\Psi_z$  are real. Thus, the contributions of the different Cartesian core-hole configurations to  $\Gamma_{if}$  are uncoupled and Eq. (5) may be rewritten as

$$\Gamma_{if} = 2\pi \sum_{\alpha}^{x,y,z} |C_{i,\alpha}|^2 \sum_{lm} |\langle \Psi_{\alpha} | \hat{H} - E | \mathcal{A} \Psi_f \varphi_c^{lm} \rangle|^2. \quad (6)$$

For simplicity the Cartesian basis configurations can be substituted now by the primitive Cartesian  $2p^{-1}$  configurations [e.g.,  $(2p_x\alpha)^{-1}$ ,  $(2p_y\alpha)^{-1}$ , and  $(2p_z\alpha)^{-1}$ ]. In the following we also neglect the generally small energy dependence of the Auger matrix elements. Thus, the decay rate of the  $i$ th core hole state is the sum of the rates of the primitive  $2p^{-1}$  configurations weighted by the  $|C_{i,\alpha}|^2$ 's which are the  $\mathcal{D}$  discussed in the preceding section.

In this work we will use a common orthogonal set of orbitals for the intermediate and final-state wave functions. The  $E$  term can now be dropped from Eq. (6) and the matrix element at the right-hand-side reduces to a sum of two electron matrix elements

$$\langle \Psi_\alpha | \hat{H} - E | \mathcal{A} \Psi_{f\mu} \varphi_c^{lm} \rangle = \sum_{v,w} \gamma_{v,w}^{\alpha f} \langle \varphi_\alpha \varphi_c^{lm} | \varphi_v \varphi_w \rangle, \quad (7)$$

where  $\varphi_v$  and  $\varphi_w$  are valence orbitals and  $\varphi_\alpha$  is the  $2p_\alpha$  core orbital.  $\gamma_{vw}^{\alpha f}$  is the two-electron transition density matrix between the intermediate state configuration  $\Psi_\alpha$  and the final-state wave function. As in our previous work [35] we approximate the valence orbitals by a linear combination of the occupied atomic orbitals ( $\chi_\mu$ )

$$\varphi_i = \sum_\mu c_{\mu,i} \chi_\mu. \quad (8)$$

Here the index  $\mu$  is running over all atomic orbitals of the molecule, which are, e.g., for HCl the  $1s$ ,  $2s$ ,  $2p_x$ ,  $2p_y$ ,  $2p_z$ ,  $3s$ ,  $3p_x$ ,  $3p_y$ ,  $3p_z$  orbitals of chlorine and the  $1s$  orbital of  $H$ . The orbital expansion coefficients  $c_{\mu,i}$  are found by projection of the valence orbitals on the basis of the atomic orbitals [35]. This leads to the matrix elements

$$\langle \varphi_\alpha \varphi_c^{lm} | \varphi_v \varphi_w \rangle = \sum_{\mu,\nu} c_{\mu,v} c_{\nu,w} \langle \chi_\alpha \varphi_c^{lm} | \chi_\mu \chi_\nu \rangle. \quad (9)$$

The integral at the right-hand side of Eq. (9) is evaluated according to the ‘‘one center approximation’’ [6], which means that (i) the continuum wave function  $\varphi_c^{lm}$  is assumed to be identical to that of the atomic case; (ii) all matrix elements that contain one or more atomic orbitals of another

atom than the core-hole atom are neglected; and (iii) the remaining matrix elements are obtained from readily available radial integrals and corresponding angular factors. The numerical values of the radial integrals were taken from the work of Chelkowska and Larkins [5]. These are averaged values of the radial Auger decay integrals of Chen *et al.* [36], which were calculated by a multiconfiguration Dirac-Fock method using the bound orbitals of the intermediate state and the Coulomb operator as the two-electron operator.

### C. Auger line shapes

The line shapes for the HCl Auger electron spectrum were described by the moment method of Cederbaum and Tarantelli [37]. In this theory the ground ( $0$ ), intermediate ( $i$ ), and final ( $f$ ) state potential energy curves are assumed to be parabolas with the curvature of the ground-state potential energy curve but different local and energetical positions. The envelopes of the vibrational features are simulated by Gaussian functions. The energetical position  $P_\mu$  and width  $W_\mu$  [full width at half maximum (FWHM)] of the Gaussian function for the  $\mu$ th final state are given by

$$P_\mu = E_c - E_{f\mu} - \frac{E'_c(E'_c - E'_{f\mu})}{E''_0} \left( 1 - \frac{\Gamma^2}{\Gamma^2 + \omega^2} \right) \quad (10)$$

and

$$W_\mu = \sqrt{8 \ln 2 \frac{(E'_c - E'_{f\mu})^2}{2E''_0} \left\{ \omega + \frac{E'^2_c}{E''_0} \left[ 1 + \frac{\Gamma^2}{\Gamma^2 + 4\omega^2} - 2 \left( \frac{\Gamma^2}{\Gamma^2 + \omega^2} \right)^2 \right] \right\} + W_{\text{expt}}^2}, \quad (11)$$

where  $E$ ,  $E'$ , and  $E''$  are the energies and the first and second derivatives of the potential energy curves at the Franck-Condon point.  $\omega$  is the ground-state vibrational frequency and  $\Gamma$  the total decay rate of the core ionized state.  $W_{\text{expt}}$  is the FWHM of the broadening caused by the electron spectrometer. The above formalism is suitable to produce overall features of Auger-electron spectra even if a part of the final states is not bound [3], as in the case of HCl or the former treated HF example of Zähringer *et al.* [38]. The detailed vibrational structure can, however, not be obtained by this method. In this case one would have to refer to the more general lifetime vibrational interference theory [39].

### D. Computational details

The relative energies and wave functions of the final states were obtained by CI calculations [40] of several selected electronic configurations. These wave functions determine the two electron transition density matrix elements [Eq. (7)] and the orbital expansion coefficients [Eq. (8)] that are used to obtain the Auger transition rates. The final states reached in the low kinetic part of the argon and HCl Auger-electron spectra are well known to have large admixtures of correlating configurations in which one or more electrons are

excited from valence orbitals to Rydberg orbitals. The orbitals, which were used to set up the configurations of the CI, were designed to be optimal for a balanced description of all final states. Thus valence orbitals generated by a CASSCF [41] method for an average of all two-hole configurations in the valence space and Rydberg orbitals from a modified virtual orbital technique [42] using the averaged Fock operator of all three-hole configurations within the prior valence orbitals were used. The CI space included all two-hole configurations and some single and double excitations from them into the first Rydberg orbitals.

For argon we used the  $16s11p3d$  basis functions of the correlation consistent polarized valence quadruple zeta (cc-pVQZ) basis set by Woon and Dunning [43], but we released their contraction substantially to  $10s9p3d$ . Two extra sets of  $d$  functions with exponents 11.7 and 4.68 were added. These are needed for an accurate description of the  $3d$  orbitals in  $\text{Ar}^{2+}$ . Furthermore, the following flat basis functions with exponents according to the recipe of Kaufmann *et al.* [44] were added in order to describe Rydberg orbitals correctly: Five  $s$  functions (exponents 0.100, 0.053, 0.030, 0.018, and 0.012), four  $p$  functions (exponents 0.090, 0.051, 0.031, and 0.020), and four  $d$  functions (exponents 0.128, 0.073, 0.044,

and 0.029). This basis set is adequate for a description of  $s$ ,  $p$ , and  $d$  Rydberg orbitals up to an effective quantum number ( $n_{\text{eff}}$ ) of 4.5. For the more accurate calculations with the multiconfiguration coupled electron pair approach (MCCEPA) [45] two sets of  $f$  functions with exponents 0.543 and 1.325 [43] were also included.

The basis set for the Cl atom of HCl was chosen similar to that of argon: The  $16s11p3d$  primitive basis set of the cc-pVQZ basis was contracted to  $11s9p3d$  and augmented by two sets of  $d$  orbitals (exponents 9.462, 3.831). Rydberg basis functions up to  $n_{\text{eff}}=4.0$  ( $s$ : 0.100, 0.053, 0.030, and 0.018;  $p$ : 0.179, 0.090, 0.051, 0.031;  $d$ : 0.128, 0.073, and 0.044) and one  $f$  set (exponent 0.706 [43]). For the hydrogen atom we used a  $6s1p/3s1p$  basis [43]. If not stated otherwise, the calculations for the HCl molecule were performed at the experimental equilibrium distance of its ground state ( $r_e = 2.40850a_0$  [46]). The coordinate system is chosen such that the H-Cl bond is on the  $z$  axis.

For the  $L_{2,3}VV$  Auger-electron spectra two different energy scales will be used below: kinetic energies, which correspond more directly to the spectral features, and binding energies, which are well-defined single numbers for each final state, whereas each final state appears in the Auger-electron spectrum with (at least) two kinetic energies. As shown in our prior work [3,47] the MCCEPA method provides absolute theoretical energies for both scales with an accuracy of about 0.1 eV. But, absolute theoretical energies compare differently to experimental data on the kinetic and binding energy scale. In order to simplify this comparison, the theoretical final-state energies were shifted to the experimental values of the lowest final states.

#### IV. THE $L_{2,3}MM$ AUGER-ELECTRON SPECTRUM OF ARGON

Previously, the  $L_{2,3}MM$  Auger-electron spectrum of argon has been studied extensively both experimentally and theoretically (see Pulkkinen *et al.* [32] and references therein, and Vikor *et al.* [48]). The spin-orbit splitting between the  $L_2$  and  $L_3$  core-hole states is 2.15 eV while the fine-structure splitting in the final states is of the order of the natural linewidth of the core-ionized state (0.11 eV [49]). Calculations by McGuire [50], Dyall and Larkins [51], Kvalheim [4], and recently by Pulkkinen *et al.* [32] have indicated the importance of the final ionic state configuration interaction (FISCI). Our test calculations for argon are not meant to compete with these previous, more sophisticated studies, but rather to show how reliably the parameters of the current calculations were chosen.

The final states were obtained from CI calculations including the diagram configurations  $(3s3p)^{-2}$  and the excited configurations  $(3s3p)^{-3} (3d,4s,4p,4d,5s)^1$  and  $(3s3p)^{-4} (3d,4s)^2$  in the configuration space. Also calculations with excitations to higher Rydberg orbitals were made, but this did not lead to a clear improvement of the calculated spectra. The energetical positions of the strongest lines were also calculated by the MCCEPA method. In Fig. 1 we present the experimental argon  $L_{2,3}MM$  spectrum of Pulkkinen *et al.* [32] together with our calculations. Table II shows experimental and calculated details of the peaks labeled in Fig. 1.

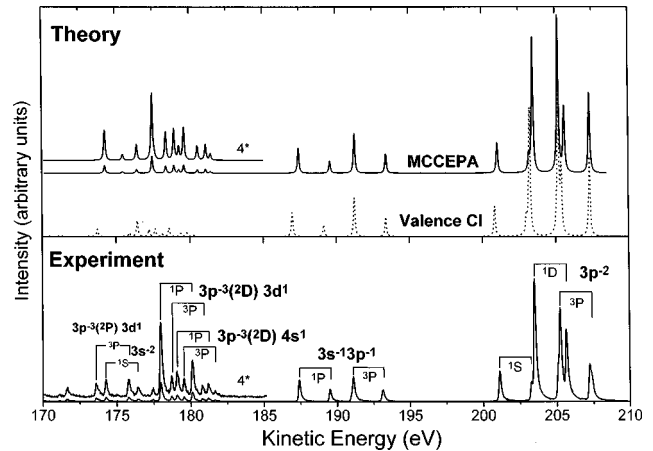


FIG. 1. Experimental argon  $L_{2,3}MM$  Auger-electron spectrum together with the calculated spectra that were generated using valence CI or MCCEPA energies for the final states. The most intensive peaks are labeled. The energy of the spectra was adjusted to the  $^3P$  line at 207.32 eV.

General features of the experimental spectrum are well reproduced by the nonrelativistic calculations. As in former theoretical studies, the line positions in the kinetic energy region between 185 and 210 eV ( $3s^{-1}3p^{-1}$ , and  $3p^{-2}$  states), which is free from correlation satellite structures, are reproduced by the valence CI method with an average deviation from the experimental energies of 230 meV. The MCCEPA method yields clearly more accurate energies with average deviations of 90 meV, indicating the need for the accurate treatment of the electron correlation. The line intensities correlate well with previous theoretical studies. As in these prior studies, our theoretical  $^3P$  to  $^1D$  intensity ratio deviates remarkably from the experimental one. We should note that the correct ratio has not been obtained with the most sophisticated methods [52], where the final continuum state configuration interaction (FCSCI) was included in multiconfiguration Dirac-Fock (MCDF) calculations.

The low kinetic energy region (below 185 eV) is, on the other hand, dominated by a manifold of correlation satellite structures. In this energy region we also obtained intensities with reasonable agreement with experiment but the valence CI method underestimates the kinetic energies by about 1.5 eV. This is due to the limited CI space, of up to about 1000 configurations per symmetry, which was used for the present calculations. The MCCEPA approach, on the other hand, describes electron correlation more precisely and, thus, gives energetical positions with an improved average accuracy of 0.23 eV.

It should be noted here that such an accuracy is desirable for theoretical Auger-electron spectra but generally not necessary for correct assignments. Furthermore, the high level MCCEPA calculations are rather time consuming for other than the  $3p^{-2}$  states. Therefore, we did not apply the MCCEPA method for the final-state energies of HCl, where they would be (i) even more cumbersome due to the increased number of final states per symmetry and the additional degree of freedom along the bond axis and (ii) less required due to the dissociative nature of most final states.

Our result for the natural linewidth of the  $2p^{-1}$  core hole state is  $5.55 \times 10^{-3}$  a.u. (0.15 eV). This value is about 37  $\pm$

TABLE II. Calculated and experimental energies and intensities of the  $L_{2,3}MM$  Auger-electron spectrum of Ar. The intensities are normalized by setting the total intensity of the  $3p^{-2}$  states to 100. Experimental energies and intensities are taken as an average value from the  $L_2$  and  $L_3$  transitions from Ref. [32]. The calculated total energy of the  $3p^{-2}(^3P)$  state is given in brackets. The number in parentheses in the last column is the contribution of the  $3s^{-1}3p^{-1}$  configuration to the wave function in percent.

Energy relative to $3p^{-2}(^3P)$ in eV			Intensity			
Valence CI	MCCEPA	Expt.	Valence-CI	Expt.	Term	Leading configuration
Diagram lines						
(-14296.50)	(-14298.95)	0.00	49.0	42.4	$^3P$	96% $3p^{-2}$
1.93	1.73	1.67	41.5	45.9	$^1D$	95% $3p^{-2}$
4.32	4.14	4.06	9.5	11.8	$^1S$	92% $3p^{-2}$
13.92	13.89	14.17	12.1	10.4	$^3P$	75% $3s^{-1}3p^{-1}$
18.18	17.72	17.78	7.5	8.4	$^1P$	44% $3s^{-1}3p^{-1}$
31.41	30.90	30.90	2.4	1.5	$^1S$	40% $3s^{-2}$
Correlation satellite lines						
27.06	25.88	25.65	1.0	1.6	$^3P$	70% $3p^{-3}4s^1$ (6)
27.52	26.25	26.11	2.4	2.5	$^1P$	71% $3p^{-3}4s^1$ (14)
27.95	26.80	26.49	2.2	1.9	$^3P$	52% $3p^{-3}3d^1$ (13)
28.73	27.69	27.24	5.1	6.7	$^1P$	34% $3p^{-3}3d^1$ (30)
31.91	29.76	29.38	0.5	1.2	$^1P$	78% $3p^{-3}3d^1$ (3)

12% higher than the corresponding experimental value of  $0.11 \pm 0.01$  eV [49]. As shown by Tulkki *et al.* [53] the calculated total decay rate depends very sensitively on the choice of the wave functions. They found that frozen-core total  $L_{2,3}$  Auger decay rates calculated with intermediate state orbitals are larger than the experimental values. In the present work, radial integrals calculated with intermediate state orbitals [36] were used. Thus, our calculations can be expected to overestimate the total decay rate. In addition, because we know that radial integrals do not change remarkably for chlorine as compared to argon, we might expect that the total decay rate is also overestimated for chlorine.

The test calculations demonstrated that the  $L_{2,3}MM$  Auger electron spectrum of argon was calculated with relatively good accuracy compared to the experimental spectrum. This agreement gives us an opportunity to move one step further—to the  $L_{2,3}VV$  spectrum of HCl. Before we can do so, we first have to consider the nonisotropical core hole density distribution of the HCl intermediate states.

### V. MOLECULAR-FIELD SPLITTING OF THE HCIL ( $2p^{-1}$ ) STATES

The nonrelativistic ionization energies of the  $2p_z^{-1}$  and the two degenerate  $2p_x^{-1}$  and  $2p_y^{-1}$  states were calculated on different levels of accuracy. In Table III we present the average ionization potentials and the splitting of the  $^2\Pi_{3/2}$  and  $^2\Sigma_{1/2}^+$  states that result from the inclusion of the spin-orbit interaction according to Eq. (3) with  $\gamma=1.08$  eV. The latter value can be obtained from experimental data [18] or from the relativistic calculations of Ellingsen *et al.* [20]. Furthermore, also the core hole densities are included in Table III.

As shown in prior work of Børve *et al.* [15,19] and Ellingsen *et al.* [20], Koopmanns theorem yields relatively poor agreement with experiment to both ionization energies and molecular-field splitting. The former is substantially improved when relaxation of the orbitals in the core ionized

state is included by the  $\Delta$ SCF approach, but the correct splitting due to the molecular field is reached only if electron correlation effects are included. This was done here by the MCCEPA method with explicit inclusion of all single and double excitations from all occupied orbitals into the virtual and partially occupied orbitals that do not increase the number of electrons in the  $2p$  orbitals. Here SCF reference wave functions were used for both the ground and the core-ionized states. It was shown before that such a CI-type calculation gives nonrelativistic  $2p$  ionization potentials that compare favorably to experimental data after inclusion of the spin-orbit splitting [15,19].

TABLE III. Averaged ionization potentials ( $\mathcal{V}_{av}$ ), molecular field splitting of the  $2p_{3/2}^{-1}$  states ( $\Delta E(^2\Pi_{3/2} - ^2\Sigma_{1/2}^+)$ ), and the  $2p_z$  core-hole densities ( $\mathcal{D}_z$ ) in the  $^2\Sigma_{1/2}^+$  and  $^2\Pi_{1/2}$  states.  $\mathcal{D}_z$  of the  $^2\Pi_{3/2}$  states is 0.00 and the  $2p_x$  and  $2p_y$   $\mathcal{D}$ 's of all states are  $\frac{1}{2}(1 - \mathcal{D}_z)$ .

Method	$\mathcal{V}_{av}$ (eV)	$\Delta E(^2\Pi_{3/2} - ^2\Sigma_{1/2}^+)$ (meV)	$\mathcal{D}_z$	
			$^2\Sigma_{1/2}^+$	$^2\Pi_{1/2}$
Koopmanns	218.82	33.1	0.65	0.35
$\Delta$ SCF <sup>a</sup>	207.57	35.0	0.65	0.35
MCCEPA <sup>a</sup>	207.74	92.0	0.63	0.37
Vibrations <sup>a,b</sup>	207.71	87.4		
MCCEPA <sup>c</sup>	207.86	83.7	0.63	0.37
Relativistic CI <sup>d</sup>	207.54	78	0.65	0.37
Expt. <sup>e</sup>	207.95	$79 \pm 8$		

<sup>a</sup>Basis as described in Sec. III D.

<sup>b</sup>Including zero point vibrational effects with MCCEPA energies.

<sup>c</sup> $16s11p5d1f/12s10p5d1f$  basis as described in Sec. III D plus two additional  $d$  sets (exponents: 70 and 25), two  $f$  sets (8 and 2.4), and one  $g$  set (0.827).

<sup>d</sup>Relativistic valence and core CI including the Davidson correction [20].

<sup>e</sup>Reference [18].

According to Table III the molecular-field splitting between the  $2p_{3/2}^{-1}$  states is slightly overestimated by the current single-point calculations. As the splitting of the  $2p^{-1}$  states is likely to depend on the internuclear distance, we included zero-point vibrational effects using potential-energy curves that were obtained by diagonalization of the matrix in Eq. (3) with MCCEPA energies for the nonrelativistic  $2p^{-1}$  states. This diminishes the  $2p_{3/2}^{-1}$  molecular field splitting by 4.5 meV, which is smaller than the experimental error estimate. The average MCCEPA ionization energy is about 0.2 eV too small. An extension of the basis set to a  $16s11p7d3f1g/11s9p7d3f1g$  basis with reasonably chosen exponents for the description of the electron correlation within the core orbitals reduces this deviation to about 0.1 eV. Further reduction of this value can be expected by improvements of the basis set and by explicit inclusion of the valence ionized states in the correlation space of the MCCEPA method. Nevertheless, much better agreement to the experimental ionization energies would be incidental, as corrections on the order of 0.1 eV [54] have to be expected from the continuum bound state interactions that cannot be properly taken into account in the CI treatment.

Table III shows that the results of the present calculations are also in good agreement with the results of the relativistic calculations of Ellingsen *et al.* [20]. The differences in the ionization potentials and the molecular-field splitting are most probably due to different choices of the CI space and the basis sets. The core hole densities of the single point large basis MCCEPA calculations were used for the calculation of the HCl Auger transition rates.

## VI. $L_{2,3}VV$ AUGER-ELECTRON SPECTRUM OF HCl

As in the calculations of the argon  $L_{2,3}MM$  Auger-electron spectrum, we can expect that configurations that involve the lowest virtual orbitals have a substantial influence on the energetical spacing and the distribution of the final states. From the photoabsorption spectra of HCl [27] it is well known that the lowest virtual orbital is not a typical Rydberg orbital but the antibonding  $6\sigma^*$  valence orbital. This led to our choice of the configuration space of the final-state CI. The following configurations with respect to the ground-state electron configuration  $1\sigma^2 2\sigma^2 3\sigma^2 1\pi^4 4\sigma^2 5\sigma^2 2\pi^4$  of HCl were used. Beside the diagram configurations, which have two holes in the valence orbitals ( $4\sigma$ ,  $5\sigma$ , and  $2\pi$ ), also single and double excitations from these orbitals to the  $6\sigma^*$  and  $3d$  orbitals, and single excitations to the higher  $4s$ ,  $4p$ ,  $4d$ , and  $5s$  Rydberg orbitals were included. As in the case of argon, further expansions of the CI space did not cause significant changes in the theoretical spectrum.

The data needed for the simulation of the envelopes of the vibrational structures by the moment method [37] were obtained as follows. All energies and the Auger intensities were calculated at the equilibrium bond distance of the ground state ( $r_e = 2.40850a_0$  [46]). The energy derivatives for the final and core ionized states were obtained by numerical differentiation. The HCl ground-state vibrational frequency ( $2989.7 \text{ cm}^{-1}$ ) was taken from the experiment [46]. The slopes ( $E'_c$ ) of the potential energy curves (PECs) of the core-ionized intermediate states were almost equal for all

states. Thus, we used an average value of  $-0.24 \text{ eV}/a_0$  in our calculations. The slopes of the final states are smaller throughout, between  $-1.9 \text{ eV}/a_0$  and  $-8 \text{ eV}/a_0$  as indicated in Table IV. General trends of these slopes may be rationalized from the occupation of the orbitals. For instance, the  $^3\Sigma^-$ ,  $^1\Delta$ , and  $^1\Sigma^+$  states with two holes in the nonbonding  $2\pi$  orbital are more strongly bound than the states with holes in the bonding  $5\sigma$  orbital or electrons in the strongly antibonding  $6\sigma^*$  orbital. This simple picture is only qualitatively correct as configuration mixing and avoided crossings have also substantial effects on the form of the PECs.

In Table IV the results of the present calculations are collected and compared to previous calculations by Kvalheim [4], and Chelkowska and Larkins [5]. In Fig. 2 we compare our theoretical spectrum with the experimental one. The lowest binding energy part of the spectrum (35–47 eV) is composed of  $(5\sigma 2\pi)^{-2}$  states, which obtain about 73% of the total Auger decay intensity. The calculated energetical positions of the lines in this region are in good agreement with the experiment. The rest of the total intensity is distributed among the  $4\sigma^{-1} 2\pi^{-1}$ ,  $4\sigma^{-1} 5\sigma^{-1}$ , and  $4\sigma^{-2}$  configurations, which mix strongly with correlation satellite configurations. As for argon, the binding energies of these states are underestimated approximately by 2 eV. Thus, the theoretical spectrum seems to be “stretched” as compared to the experimental one. In Table IV we indicated the strongest diagram configuration even for those states where they are not the leading configurations. Due to the choice of the intermediate state wave function in our calculations, only the contributions of diagram configurations to a state give rise to Auger intensity.

So far we have not considered the contribution of shakeup transitions in the intermediate states to our experimental spectrum. Calculations of Carravetta and co-workers [31] indicate that shakeup and shakeoff states contribute with 11% and 8%, respectively, to the ionization cross section. With a more approximate approach Kochur *et al.* obtained a value of 12.8% for the total shake cross section [8]. According to the work of Kochur *et al.* [8] the shake states give rise to broad structures in the Auger-electron spectrum, which are mainly located between 163- and 159-eV kinetic energy. Indeed, the experimental spectrum shows structures in that region that cannot be found in the theoretical spectrum. Furthermore, our calculations predict that 69% of the total Auger intensity appear above 165-eV kinetic energy, whereas in the experimental spectrum 57% of the total intensity belongs to this region. Assuming the theoretical ratio to be exact for the decay of the  $2p^{-1}$  states and the shake satellite structures to appear exclusively below 165-eV kinetic energy, this results in a total shake intensity of 20%, which agrees well with the best theoretical value (19%) of Carravetta *et al.* [31].

In Table V we compare calculated intensities for the decay of the different intermediate states to the  $(5\sigma 2\pi)^{-2}$  final states with the experimental work of Aksela *et al.* [18]. In their work the form of the vibrational fine structure in the Auger lines was assumed to be identical for all  $2\pi^{-2}$  final states and was determined from the  $2p^{-1}(^2\Pi_{1/2}) \rightarrow ^3\Sigma^-$  line. The calculations predict an intensity ratio of 1.6:0.6:1.0 for the transitions from the  $^2\Pi_{3/2}$ ,  $^2\Sigma_{1/2}^+$  and  $^2\Pi_{1/2}$  intermediate states to both the  $^3\Sigma^-$  and  $^1\Delta$  final states. This is in a

TABLE IV. Computed data for HCl. Rows from left to right: Position of the binding energy center of the peak ( $P_\mu$ ) in eV, energy derivative ( $E'_{f\mu}$ ) in eV/ $a_0$ , Gaussian FWHM ( $W_\mu$ ) in eV, and decay rates from the  $2p_{3/2}^{-1}(^2\Pi_{3/2})$ ,  $2p_{3/2}^{-1}(^2\Sigma_{1/2}^+)$ , and  $2p_{1/2}^{-1}(^2\Pi_{1/2})$  states in  $10^{-4}$  a.u. The term symbols and the leading configuration are given in the next two columns. The four rightmost columns include the calculated binding energies ( $E$ ) in eV and intensities ( $I$ ) in  $10^{-4}$  a.u. of Kvalheim [4] and Chelkowska and Larkins [5]. As absolute intensities were not given in Ref. [4], we normalized these intensities to our average total intensity. The contribution of the diagram configurations in some energy levels is designated by ( $xw$ ), where  $x=a, b$ , and  $c$  denote diagram configurations  $4\sigma^{-1}2\pi^{-1}$ ,  $4\sigma^{-1}5\sigma^{-1}$ , and  $4\sigma^{-2}$ , respectively.  $w$  is the contribution of this configuration in percent.

$P_\mu$	$E'_{f\mu}$	Present work				Term	Leading configuration	Ref. [4]		Ref. [5]	
		$W_\mu$	$^2\Pi_{3/2}$	$^2\Sigma_{1/2}^+$	$^2\Pi_{1/2}$			$E$	$I$	$E$	$I$
35.64	-1.90	0.57	9.21	3.41	5.08	$^3\Sigma^-$	95% $2\pi^{-2}$	35.7	4.69	35.7	7.06
37.42	-1.85	0.56	9.19	3.64	5.94	$^1\Delta$	95% $2\pi^{-2}$	37.5	6.62	37.0	7.20
38.76	-1.89	0.57	4.95	1.94	3.19	$^1\Sigma^+$	92% $2\pi^{-2}$	38.7	3.26	38.3	4.51
39.50	-3.79	1.21	6.69	9.91	8.54	$^3\Pi$	95% $5\sigma^{-1}2\pi^{-1}$	39.6	9.27	37.9	7.60
41.08	-4.42	1.43	3.63	5.09	4.48	$^1\Pi$	94% $5\sigma^{-1}2\pi^{-1}$	41.2	6.52	38.8	3.94
46.21	-6.07	1.99	0.22	3.30	2.03	$^1\Sigma^+$	88% $5\sigma^{-2}$	46.3	3.67	43.5	1.25
48.33	-4.76	1.54	2.54	1.11	1.70	$^3\Pi$	44% $4\sigma^{-1}2\pi^{-1}$	49.0	1.55	50.8	4.41
49.62	-5.66	1.85	0.52	0.20	0.33	$^1\Pi$	73% $2\pi^{-3}6\sigma^{*1}$ ( $a^9$ )	50.4	0.26		
50.06	-5.29	1.72	1.54	0.70	1.05	$^3\Pi$	53% $2\pi^{-3}6\sigma^{*1}$ ( $a^{27}$ )	50.8	0.76		
51.09	-7.13	2.35	0.00	0.74	0.43	$^3\Sigma^-$	58% $5\sigma^{-1}2\pi^{-2}6\sigma^{*1}$ ( $b^{29}$ )	52.0	0.52		
53.52	-5.52	1.80	2.06	0.79	1.32	$^1\Pi$	35% $4\sigma^{-1}2\pi^{-1}$	54.4	1.48	56.4	4.51
54.09	-6.18	2.02	0.00	1.08	0.63	$^3\Sigma^-$	42% $4\sigma^{-1}5\sigma^{-1}$	54.8	0.64	53.8	1.18
55.22	-5.56	1.82	0.08	0.34	0.24	$^1\Sigma^+$	31% $5\sigma^{-1}2\pi^{-2}6\sigma^{*1}$ ( $b^{18}$ )	56.3	0.31		
57.12	-5.95	1.95	0.10	0.32	0.22	$^1\Sigma^+$	34% $5\sigma^{-1}2\pi^{-2}3d^1$ ( $b^{16}$ )				
59.61	-4.32	1.39	0.63	0.24	0.40	$^3\Pi$	40% $5\sigma^{-1}2\pi^{-2}3d^1$ ( $a^{11}$ )				
60.35	-4.71	1.52	1.18	0.44	0.70	$^1\Pi$	38% $2\pi^{-3}4p^1$ ( $a^{20}$ )				
60.66	-3.76	1.20	0.23	0.09	0.14	$^3\Pi$	73% $2\pi^{-3}4p^1$ ( $a^4$ )				
61.13	-4.16	1.34	1.21	0.45	0.77	$^1\Pi$	49% $2\pi^{-3}4p^1$ ( $a^{20}$ )				
62.89	-4.87	1.58	0.20	0.08	0.13	$^1\Pi$	56% $5\sigma^{-1}2\pi^{-2}3d^1$ ( $a^4$ )				
63.21	-6.37	2.09	0.00	0.34	0.20	$^3\Sigma^-$	33% $5\sigma^{-2}2\pi^{-1}3d^1$ ( $b^{13}$ )				
63.60	-4.50	1.45	0.42	0.65	0.55	$^1\Sigma^+$	27% $5\sigma^{-1}2\pi^{-2}3d^1$ ( $b^{18,c12}$ )				
63.81	-8.22	2.72	0.01	0.37	0.22	$^1\Sigma^+$	20% $4\sigma^{-1}2\pi^{-2}6\sigma^{*1}$ ( $b^{14}$ )				
66.65	-5.51	1.80	0.14	0.26	0.22	$^1\Sigma^+$	29% $2\pi^{-4}6\sigma^{*2}$ ( $c^{11}$ )				
			1.62	1.82	1.73	Other states			2.00		1.73
			46.38	37.23	41.01	Total rates			39.7		41.54

fairly good agreement with the experiment. The main disagreement between experiment and theory arises from the fact that the theory tends to overestimate the transition rates to the  $^3\Sigma^-$  state in a similar way as the  $^3P$  state is overestimated in Ar. Further, for the final state configurations  $2\pi^{-2}$ ,  $2\pi^{-1}5\sigma^{-1}$ , and  $5\sigma^{-2}$ , calculations predict relative intensity ratios for the decay from the  $^2\Pi_{3/2}^{-1}:^2\Sigma_{1/2}^+:^2\Pi_{1/2}^{-1}$  intermediate states of 1.6:0.6:1.0, 0.8:1.1:1.0, and 0.1:1.6:1.0, respectively.

We have included in Tables IV and V results from previous work by Kvalheim [4], and Chelkowska and Larkins [5]. These studies did not account for the effect of the molecular field. Instead it was assumed that the intensity ratio of the spin-orbit split components is statistical ( $2p_{3/2}/2p_{1/2}=2$ ). Further, in the work of Kvalheim FISC was included in a similar way as in our work, whereas Chelkowska and Larkins included only diagram configurations in their calculations. Therefore, our results agree much better with the study of Kvalheim. As in that work we also find that FISC has a significant effect to the spectrum.

We obtained rather different total Auger decay rates for different intermediate states. The values of 126, 99, and 113

meV were calculated for the  $2p_{3/2}^{-1}(^2\Pi_{3/2})$ ,  $2p_{3/2}^{-1}(^2\Sigma_{1/2}^+)$ , and  $2p_{1/2}^{-1}(^2\Pi_{1/2})$  core-ionized states. Our calculations most probably overestimate the total decay rate by 25–50% as they do also for argon. Experimental  $2p$  core-hole lifetime widths of  $95 \pm 15$  meV were reported by Aksela *et al.* [18]. This value may be compared with the average theoretical decay width of 113 meV. Hence, the calculated width is about  $20 \pm 20\%$  greater than the experimental one. Note that the different widths for the core-hole states cannot be confirmed by the experiment as the  $^2\Pi_{3/2}$  and  $^2\Sigma_{1/2}^+$  states are too close to each other to determine their individual widths.

## VII. DEPENDENCE OF THE TOTAL AUGER RATE ON THE $2p$ CORE-HOLE ORIENTATION

In Table VI we list the contributions of different Cartesian two-hole configurations to the total Auger decay rate of a hypothetical argon  $2p_z^{-1}$  core-hole state. This shows a pronounced correlation between the orientation of the core hole and the valence  $3p$  orbitals that participate to the most intense Auger transitions. More than 97% of the Auger intensity stems from transitions that involve the  $3p$  valence or-

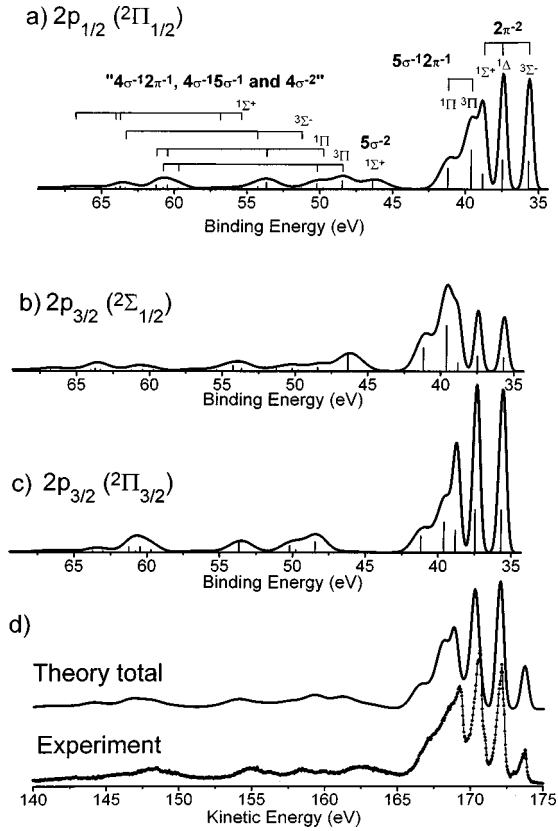


FIG. 2. Experimental and calculated  $L_{2,3}VV$  Auger-electron spectra of HCl. Calculated contributions of the (a)  $2p_{1/2}(^2\Pi_{1/2})$ , (b)  $2p_{3/2}(^2\Sigma_{1/2}^+)$ , (c)  $2p_{3/2}(^2\Pi_{3/2})$  intermediate states, and (d) the calculated total spectrum with the experimental Auger-electron spectrum.

bital with the same spatial orientation as the core hole.

This orientational correlation of the intermediate and final-state configurations was used recently as an intuitive argument for the interpretation of the intensity patterns of the HS Auger-electron spectrum [21]. Furthermore, the ratio of two intensities in Table VI (the partial intensities for the decay into the  $3p_z^{-2}$  to the  $3p_x^{-2}$  configurations) was recently used by Gel'mukhanov *et al.* [17] for the explanation of the  $2p^{-1} \rightarrow 2b_1^{-2}$  Auger decay rates of  $H_2S$ . Note, that we can take the results of Table VI as a good qualitative approximation for the evaluation of the total Auger transition

rates of HCl, as the Auger transition integrals for chlorine and argon differ only by a few percent [5]. We only have to account for the changed effective population of the corresponding molecular valence orbitals at the chlorine atom. These populations can be obtained from the atomic orbital (AO) expansion factors [see Eq. (8)] that are collected in Table VII. This table also contains the squared coefficients of the atomic valence orbitals ( $c_{\mu,i}$ ) times their occupation numbers ( $n_i$ ) summed over all molecular orbitals

$$n_{\text{occ},\mu} = \sum_i n_i c_{\mu,i}^2. \quad (12)$$

We designate these numbers as atomic occupation numbers. They represent the occupation number of the atomic orbitals that is felt at (or near to) the atomic nucleus. In order to obtain the total transition rate of the  $2p_z$  core hole, we have to multiply each of the two hole configurations in Table VI by the degeneracy and the atomic occupation numbers of these two holes. Table VI shows that the only chlorine atomic orbital with an atomic occupation number smaller than two is the  $3p_z$  orbital.

This is due to a fundamental property of chemical bonds. For the case of the HCl molecule we may explain this for the bonding orbital ( $\varphi_b$ )

$$\varphi_b = c_{3p_z,b} \chi_{3p_z} + c_{1s,b} \chi_{1s}, \quad (13)$$

where the indices  $3p_z$  and  $1s$  stand for the chlorine  $3p_z$  and hydrogen  $1s$  orbitals, respectively. The  $\chi$ 's represent the normalized atomic orbitals as introduced in Eq. (8). (A detailed analysis shows that the chlorine  $3s$  orbital is fully occupied and has a net nonbonding effect. Therefore and for the sake of simplicity, we do not consider the chlorine  $3s$  orbital in the discussion of the chemical bond.) The electron density  $\varphi_b^2$  of one electron in this orbital is distributed on three terms as

$$\int \varphi_b^2 d^3r = 1 = c_{3p_z,b}^2 + c_{1s,b}^2 + 2c_{3p_z,b}c_{1s,b} \underbrace{(\chi_{3p_z} | \chi_{1s})}_S. \quad (14)$$

According to the ideas of Mullikens population analysis, the first two terms on the right-hand side of this equation designate the electron net AO population of the chlorine  $3p_z$  and

TABLE V. Calculated and experimental partial Auger decay rates from the  $2p_{3/2}(^2\Pi_{3/2})$ ,  $2p_{3/2}(^2\Sigma_{1/2}^+)$ , and  $2p_{1/2}(^2\Pi_{1/2})$  core-ionized states to the  $(5\sigma 2\pi)^{-2}$  final states of HCl. The two rightmost columns contain calculated intensities by Kvalheim [4] and Chelkowska and Larkins [5]. The intensities are normalized with respect to the  $2p_{1/2}(^2\Pi_{1/2}) - 2\pi^{-2}(^3\Sigma^-)$  line.

Term	Configuration	Experiment Ref. [18]			Present calculations			Previous calculations	
		$^2\Pi_{3/2}$	$^2\Sigma_{1/2}^+$	$^2\Pi_{1/2}$	$^2\Pi_{3/2}$	$^2\Sigma_{1/2}^+$	$^2\Pi_{1/2}$	Ref. [4]	Ref. [5]
$^3\Sigma^-$	$2\pi^{-2}$	1.60	0.80	1.00	1.59	0.59	1.00	1.00	1.00
$^1\Delta$	$2\pi^{-2}$	1.90	1.00	1.40	1.58	0.63	1.02	1.41	1.02
$^1\Sigma^+$	$2\pi^{-2}$			0.70	0.85	0.34	0.55	0.70	0.64
$^3\Pi$	$5\sigma^{-1}2\pi^{-1}$				1.15	1.71	1.47	1.98	1.08
$^1\Pi$	$5\sigma^{-1}2\pi^{-1}$				0.63	0.88	0.77	1.39	0.56
$^1\Sigma^+$	$5\sigma^{-2}$				0.04	0.57	0.35	0.78	0.18

TABLE VI. Auger transition rates ( $\Gamma_\mu$ ) for a hypothetical  $2p_z^{-1}$  state of the argon atom into final-state configurations with two holes in the Cartesian  $3s$  and  $3p$  orbitals. The atomic diagram states that correspond to the two-hole configurations are also indicated. Symmetry equivalent configurations [e.g.,  $(3p_x^{-1} 3p_z^{-1})$  and  $(3p_y^{-1} 3p_z^{-1})$ ] are shown only once. Their number is given in column “weight.” The spin multiplicity of the final-state configuration is indicated as upper index.

Final-state configuration	Corresponding diagram state	Weight	$\Gamma_\mu/10^{-3}$ a.u.
$(3p_x^{-1} 3p_y^{-1})^3$	$^3P$	1	
$(3p_x^{-1} 3p_z^{-1})^3$	$^3P$	2	1.00
$(3p_x^{-1} 3p_y^{-1})^1$	$^1D$	1	0.02
$(3p_x^{-1} 3p_z^{-1})^1$	$^1D$	2	0.49
$(3p_x^{-2})^1$	$^1D$ and $^1S$	2	0.02
$(3p_z^{-2})^1$	$^1D$ and $^1S$	1	1.11
$(3p_x^{-1} 3s^{-1})^3$	$^3P$	2	0.00
$(3p_z^{-1} 3s^{-1})^3$	$^3P$	1	0.64
$(3p_x^{-1} 3s^{-1})^1$	$^1P$	2	0.00
$(3p_z^{-1} 3s^{-1})^1$	$^1P$	1	0.66
$(3s^{-2})^1$	$^1S$	1	0.07
All configs.			5.52 (100%)
Two holes in $3p_z$			1.11 (20%)
One hole in $3p_z$			4.30 (78%)
No hole in $3p_z$			0.14 (2%)

hydrogen  $1s$  orbitals, respectively. The last term is interpreted as the overlap population between the  $3p_z$  and  $1s$  orbitals, which is the part of the electron density that is contributing to the chemical bond. It includes the overlap between the chlorine  $3p_z$  and the hydrogen  $1s$  orbitals ( $S \approx 0.5$ —a typical value for bound atomic orbitals) which is by far not negligible. According to the ideas of the one-center approximation only the net AO population of the chlorine  $3p_z$  orbital contributes to the Auger transition rates [compare Eq. (9)]. Therefore, molecular Auger-electron spectra can be considered to monitor either the net atomic populations (in the case of the HCl molecule  $c_{3p_z,b}^2$ ) or the equivalent property

$$c_{3p_z,b}^2 = 1 - c_{1s,b}^2 - 2c_{3p_z,b}c_{1s,b}S, \quad (15)$$

which is connected to the net charge carried by the bond partner—a property that can be estimated from the electronegativity of the involved atoms—and the bond strength—a highly demanding property.

The total Auger transition rate ( $\Gamma$ ) is correctly evaluated by summing the partial transition rate in Eq. (4) over all final

TABLE VII. Atomic orbital expansion factors and atomic occupation numbers of the valence orbitals of HCl.

Atomic orbital	$4\sigma$	$5\sigma$	$2\pi$	$n_{\text{occ}}$
Cl $3s$	0.94470	0.33156	0.00000	2.00
Cl $3p_{x,y}$	0.00000	0.00000	1.00000	2.00
Cl $3p_z$	-0.13164	0.81292	0.00000	1.36
H $1s$	0.08599	-0.29112	0.00000	0.18

TABLE VIII. Distribution of the HCl valence orbital electron density depending on the description of the electronic wave function. The atomic net population numbers  $n_{\text{occ}}$  of the chlorine and the hydrogen orbitals and the overlap population density (OPD) are presented as well as the total Auger transition rates  $\Gamma$  in  $10^{-3}$  a.u. for the three core-ionized states that result from Eq. (16).

	HCl $^{2+}$ <sup>a</sup>	HCl ( $2p^{-1}$ ) <sup>b</sup>	HCl ( $2p^{-1}$ ) <sup>c</sup>	HCl(X) <sup>d</sup>
$n_{\text{occ}}$ Cl( $3s$ )	2.00	2.02	2.03	1.94
$n_{\text{occ}}$ Cl( $3p_{x,y}$ )	2.00	2.00	2.00	2.00
$n_{\text{occ}}$ Cl( $3p_z$ )	1.36	1.39	1.37	1.06
$n_{\text{occ}}$ H( $1s$ )	0.18	0.17	0.23	0.40
OPD	0.46	0.42	0.37	0.60
$\Gamma(^2\Pi_{3/2})$	5.04	5.07	5.05	4.81
$\Gamma(^2\Sigma_{1/2}^+)$	4.17	4.23	4.19	3.55
$\Gamma(^2\Pi_{1/2})$	4.53	4.58	4.55	4.07

<sup>a</sup>CASSCF wave function optimized for an average of the  $(5\sigma 2\pi)^{-2}$  two-hole diagram configurations.

<sup>b</sup>SCF wave function optimized for the  $2p_x$  or  $2p_z$  core-hole states.

<sup>c</sup>CASSCF wave function obtained with the chlorine  $3\sigma$ ,  $1\pi$ ,  $4\sigma$ ,  $5\sigma$ ,  $2\pi$ , and  $6\sigma$  orbitals in the active space optimized for an average of the  $2p^{-1}$  states.

<sup>d</sup>SCF wave function of the neutral HCl ground state.

states. An approximation to this can be obtained as in the work of Gel'mukhanov *et al.* [17]. For a HCl  $2p^{-1}$  state with the  $2p$  core-hole densities  $D_x$ ,  $D_y$ , and  $D_z$ , a  $3s$ ,  $3p_x$ , and  $3p_y$  atomic occupation number of 2 and the atomic occupation number of the  $3p_z$  orbital ( $2n$ ) Table VI and the conditions  $D_x = D_y$  and  $D_x + D_y + D_z = 1$  give

$$\Gamma/(\text{a.u.}) = 0.02n^2 + 1.52n + 4.00 + D_z(1.09n^2 + 2.78n - 3.84). \quad (16)$$

This equation shows that the total transition rate depends substantially on the value  $n$ . This number may not be optimally determined by the current frozen core approach that uses molecular orbitals optimized for the HCl $^{2+}$  dication with two holes averaged over all valence MOs. The most reasonable orbitals are those of the core-ionized HCl( $2p^{-1}$ ) state. Furthermore, one may argue that the effective occupation number of the atomic orbitals may be changed by correlation effects and in particular by the admixture of configurations that contain the antibonding  $6\sigma^*$  orbital.

Therefore, we investigated how atomic population numbers change if they are determined from different wave functions. In Table VIII we present effective occupation numbers of the chlorine and hydrogen atomic orbitals calculated from different wave functions of the HCl molecule. The  $2p^{-1}$  core-ionized state is represented by two different wave functions that were both optimized for an average of the three  $2p$  core-ionized states: A restricted open shell Hartree-Fock (single configuration) wave function and a CASSCF wave function, which included in the active space the  $2p$  orbitals, the valence orbitals, and the antibonding  $6\sigma^*$  orbital. For comparison Table VIII also contains the atomic occupation numbers of the neutral HCl ground state described by a closed shell Hartree-Fock wave function. Furthermore, this table also includes the total decay rates of the three core-ionized  $2p^{-1}$  states resulting from Eq. (16) and  $D_z = 0.63$ .

All atomic population numbers show that the chlorine  $3s$ ,  $3p_x$ , and  $3p_y$  orbitals are essentially doubly filled and, therefore, do not contribute to the chemical bond. For some wave functions the atomic occupation numbers of the chlorine  $3s$  become larger than two, which is an artifact of the method of determination. The atomic net population of the  $3p_z$  orbital is essentially the same for the core-hole and final-state orbitals. It is substantially smaller for the ground-state orbitals where a larger part of the electron density is located on the hydrogen atom and in the overlap population density. Therefore, the ground-state orbitals seem to overestimate the effect of the differences between the total Auger transition rates of the  $2p^{-1}$  state, predicting them for the  $2p_{3/2}$  states 18% larger and smaller than for the  $2p_{1/2}$  state. The two-hole wave function and the wave functions of the core-ionized states give consistently 10%. Therefore, ground-state wave functions seem to be not a good choice for the description of these effects.

Note that the transition rates to the final states in Table VI may not be directly used for the calculation of partial transition rates to one single final state. In such a case generally configuration mixing and therefore constructive or destructive interference of the Auger decay channels has to be considered. Nevertheless, the data in Table VI can be used as a quantitative tool for the interpretation of partial transition rates. This explains, e.g., the small transition rate for the decay of the  ${}^2\Sigma_{1/2}^+$  into the first three  $2\pi^{-2}$  final states of the HCl molecule. Here the core hole state with preferentially  $z$  orientation wants to decay by taking at least one electron out of the  $3p_z$  orbital, which is not possible for the  $2\pi^{-2}$  final states.

We should state that the information about net charges or chemical bonds is included in all Auger electron spectra. The important difference to the more frequently considered  $KVV$  spectra is that due to the orientation of the core holes in the molecular field split intermediate states and the strong orientational dependence of the Auger transition probability, these effects of the molecular bond appear here much more pronounced as an effect within one single Auger-electron spectrum.

Interestingly, all orbital sets predict that the electron density "missing" in the  $3p_z$  orbital is predominantly moving into the overlap population density and not into the net population of the hydrogen  $1s$  orbital. The relative effect of the charge transfer and the bonding nature in decreasing the chlorine  $3p_z$  net occupation number of the bonding orbital is between 1:2.6 and 1:1.5 depending on the way the wave functions are determined. So this reduction is essentially due to the chemical bond or saying this in terms of the former discussion due to the overlap of the chlorine  $3p_z$  and hydrogen  $1s$  orbitals.

We should remark that the current findings are based on the validity of the one-center approximation and on the assumption that the molecular orbitals can be well represented by a single zeta atomic orbital basis. If these approximations do not hold, e.g., if the atomic orbitals are distorted due to the molecular environment such that the Auger transition integrals change significantly, then conclusions given above may become invalid.

## VIII. SUMMARY AND CONCLUSIONS

We have outlined a theoretical approach for the accurate calculation of molecular  $L_{2,3}VV$  Auger-electron spectra. Using well-established knowledge about the importance of correlation satellite configurations in the final states of argon, we have shown that this molecular approach is capable of reproduce the normal Auger-electron spectra of argon and HCl. The largest deficiencies of both theoretical spectra and of all recent theoretical studies of the argon  $L_{2,3}MM$  Auger-electron spectrum are too high intensities for the transitions into the lowest triplet states. Thus, the largest error of the theoretical spectrum was due to the atomic input data and not due to any approximations that are necessary for molecules. We regard this as an important indication for the reliability for the "one-center approximation" which was used here for the calculation of the transition rates.

For the realistic calculation of the spectrum it was important to choose orbitals that give a good representation of the final states within the restricted CI space. We gave a simple and straightforward recipe for their determination for the present case where strong mixing with correlating configurations plays an important role for the spectrum. In the case of the argon  $L_{2,3}MM$  Auger-electron spectrum we employed the MCCEPA approach to calculate relative final-state energies for essentially all states that appear in the spectrum. For the complete spectrum average deviations from experimental data were on the order of 0.2 eV. This accuracy, which is generally not reached with atomic calculations of Auger-electron spectra, demonstrates the importance of the inclusion of dynamic electron correlation effects if accurate energies are required.

For HCl the calculations predict rather different total and partial transition rates for the molecular field and spin-orbit split intermediate states. These are explained by the partial orientation of the core holes in the intermediate states, strong differences in the net atomic populations of the valence orbitals due to the chemical bond, and the clear orientational preference of the  $L_{2,3}VV$  Auger decay for generating valence  $p$  holes with the same orientation as the core hole. The analysis showed that the effect of the chemical bond is predominantly due to the overlap of the atomic orbitals at the bound atoms. We regard it as particularly important to investigate this finding in some more detail, as this would clarify the effect of chemical bonds on Auger transition rates and on the electronic structure of molecules.

Unfortunately, the rather strong effects of the molecular field splitting on molecular Auger-electron spectra are almost completely hidden in experimental data. This is due to the generally small size of the molecular field splitting as compared to the Lorentzian broadening of the core-ionized states. Further, experimentally it was not, so far, possible to see a strong dependence of the core-hole lifetime on its orientation. We hope that this will be possible in photoelectron spectra of other compounds or in near edge x-ray-absorption fine-structure spectra. Similarly, the strong dependence of the intensity distribution in the HCl Auger-electron spectra on the core-hole orientation cannot be rigorously checked by an experiment. A possible way to see this could be to make use of the Auger resonant Raman effect, which allows one to overcome the Lorentzian linewidth broadening in the Auger-

electron spectra. Our future work will be devoted to a better understanding of these spectra, which could further check the present theoretical findings.

#### ACKNOWLEDGMENTS

One of us (M. K.) wants to thank Professor V. Staemmler and the members of his research group for kindness and hospitality during his visit in Bochum. The support of R. F. F. by a Habilitationsstipendium of the Deutsche Forschungsge-

meinschaft under Contract No. Fi 620/1-2 is gratefully acknowledged. We are also grateful for financial support from the Council for the Natural Sciences of the Academy of Finland, the Magnus Ehrnrooth foundation, Suomen Kulttuurirahaston Pohjois-Pohjanmaan Rahasto, and the Graduiertenkolleg "Dynamische Prozesse an Festkörperoberflächen—Adsorption, Reaktion, heterogene Katalyse." R. F. F. wants to thank the research group of Professor S. Aksela for financial support and for the warm and encouraging atmosphere at his visits in Oulu.

- 
- [1] F. P. Larkins, Nucl. Instrum. Methods Phys. Res. B **87**, 215 (1994).
- [2] H. Ågren, A. Caesar, and C.-M. Liegener, Adv. Quantum Chem. **23**, 1 (1992).
- [3] R. Fink, J. Chem. Phys. **106**, 4038 (1997).
- [4] O. M. Kvalheim, Chem. Phys. Lett. **98**, 457 (1983).
- [5] E. Z. Chelkowska and F. P. Larkins, At. Data Nucl. Data Tables **49**, 121 (1991).
- [6] H. Siegbahn, L. Asplund, and P. Kelfve, Chem. Phys. Lett. **35**, 330 (1975).
- [7] V. L. Sukhorukov, I. D. Petrov, B. L. Sukhorukov, and L. A. Demekhina, Khim. Fiz. **5**, 175 (1986).
- [8] A. G. Kochur, S. A. Novikov, and V. L. Sukhorukov, Chem. Phys. Lett. **222**, 411 (1994).
- [9] E. Z. Chelkowska and F. P. Larkins, J. Phys. B **24**, 5083 (1991).
- [10] F. P. Larkins, E. Chelkowska, Y. Sato, K. Ueda, and E. Shigemasa, J. Phys. B **26**, 1479 (1993).
- [11] F. Tarantelli and L. S. Cederbaum, Phys. Rev. Lett. **71**, 649 (1993).
- [12] F. Tarantelli, A. Sgamellotti, and L. S. Cederbaum, J. Chem. Phys. **94**, 523 (1991).
- [13] M. Elango, A. Ausmees, A. Kikas, E. Nõmmiste, R. Ruus, A. Saar, J. F. van Acker, J. N. Andersen, R. Nyholm, and I. Martinson, Phys. Rev. B **47**, 11 736 (1993).
- [14] Z. F. Liu, G. M. Bancroft, K. H. Tan, and M. Schachter, J. Electron Spectrosc. Relat. Phenom. **67**, 299 (1994); J. Johnson, J. N. Cutler, G. M. Bancroft, Y. F. Hu, and K. H. Tan, J. Phys. B **30**, 4899 (1997).
- [15] M. Siggel, C. Field, L. Sæthre, K. Børve, and T. D. Thomas, J. Chem. Phys. **105**, 9035 (1996).
- [16] S. Svensson, A. Ausmees, S. J. Osbourne, G. Bray, F. Gel'mukhanov, H. Ågren, A. Naves de Brito, O.-P. Sairanen, A. Kivimäki, E. Nõmmiste, H. Aksela, and S. Aksela, Phys. Rev. Lett. **72**, 3021 (1994).
- [17] F. Gel'mukhanov, H. Ågren, S. Svensson, H. Aksela, and S. Aksela, Phys. Rev. A **53**, 1379 (1996).
- [18] H. Aksela, E. Kukku, S. Aksela, O.-P. Sairanen, A. Kivimäki, E. Nõmmiste, A. Ausmees, S. J. Osbourne, and S. Svensson, J. Phys. B **28**, 4259 (1995).
- [19] K. Børve, Chem. Phys. Lett. **262**, 801 (1996).
- [20] K. Ellingsen, T. Saue, H. Aksela, and O. Gropen, Phys. Rev. A **55**, 2743 (1997).
- [21] A. Naves de Brito, S. Svensson, S. J. Osbourne, A. Ausmees, A. Kivimäki, O.-P. Sairanen, E. Nõmmiste, H. Aksela, S. Aksela, and L. J. Sæthre, J. Chem. Phys. **106**, 18 (1997).
- [22] S. Aksela, A. Kivimäki, A. Naves de Brito, O.-P. Sairanen, S. Svensson, and J. Vöyrynen, Rev. Sci. Instrum. **65**, 831 (1994); S. Aksela, A. Kivimäki, O.-P. Sairanen, A. Naves de Brito, E. Nõmmiste, and S. Svensson, *ibid.* **66**, 1621 (1995).
- [23] H. Ahola and T. Meinander, Rev. Sci. Instrum. **63**, 372 (1992); Å. Andersson, S. Werin, T. Meinander, A. Naves de Brito, and S. Aksela, Nucl. Instrum. Methods Phys. Res. A **362**, 586 (1995).
- [24] R. Nyholm, S. Svensson, J. Nordgren, and A. Flodström, Nucl. Instrum. Methods Phys. Res. A **246**, 267 (1986); S. Aksela, A. Kivimäki, R. Nyholm, and S. Svensson, Rev. Sci. Instrum. **63**, 1252 (1992).
- [25] S. J. Osbourne, A. Ausmees, J. O. Forsell, B. Wannberg, G. Gray, L. B. Dantas, S. Svensson, S. Naves de Brito, A. Kivimäki, and S. Aksela, Synch. Rad. News **7**, 25 (1994).
- [26] S. Svensson, J. O. Forsell, H. Siegbahn, A. Ausmees, G. Bray, S. Södergren, S. Sundin, S. J. Osbourne, S. Aksela, E. Nõmmiste, J. Jauhiainen, M. Jurvansuu, J. Karvonen, P. Barta, W. R. Salaneck, A. Ewaldsson, M. Lögdlund, and A. Fahlman, Rev. Sci. Instrum. **67**, 2149 (1996).
- [27] K. Ninomiya, E. Ishiguro, S. Iwata, A. Mikuni, and T. Sasaki, J. Phys. B **14**, 1777 (1981).
- [28] H. Aksela, S. Aksela, M. Hotokka, and M. Jäntti, Phys. Rev. A **28**, 287 (1983).
- [29] S. Svensson, L. Karlsson, P. Baltzer, M. Keane, and B. Wannberg, Phys. Rev. A **40**, 4369 (1989).
- [30] T. Kylli, H. Aksela, A. Hiltunen, and S. Aksela, J. Phys. B **30**, 3647 (1997).
- [31] V. Carravetta, H. Ågren, D. Nordfors, and S. Svensson, Chem. Phys. Lett. **152**, 190 (1988).
- [32] H. Pulkkinen, S. Aksela, O.-P. Sairanen, A. Hiltunen, and H. Aksela, J. Phys. B **29**, 3033 (1996).
- [33] S. Svensson, B. Eriksson, N. Mårtensson, G. Wendin, and U. Gelius, J. Electron Spectrosc. Relat. Phenom. **47**, 327 (1988).
- [34] G. C. King, M. Tronc, F. H. Read, and R. C. Bradford, J. Phys. B **10**, 2479 (1977).
- [35] R. Fink, J. Electron Spectrosc. Relat. Phenom. **76**, 295 (1995).
- [36] M. H. Chen, F. P. Larkins, and B. Crasemann, At. Data Nucl. Data Tables **45**, 1 (1990).
- [37] L. S. Cederbaum and F. Tarantelli, J. Chem. Phys. **98**, 9691 (1993).
- [38] K. Zähringer, H.-D. Meyer, L. S. Cederbaum, F. Tarantelli, and A. Sgamellotti, Chem. Phys. Lett. **206**, 247 (1993).
- [39] F. K. Gel'mukhanov, L. N. Mazalov, and A. V. Kondratenko, Chem. Phys. Lett. **46**, 133 (1977); F. Kaspar, W. Domcke, and L. S. Cederbaum, Chem. Phys. **44**, 33 (1979); N. Correia, A. Flores-Riveros, H. Ågren, K. Helenelund, L. Asplund, and U. Gelius, J. Chem. Phys. **83**, 2035 (1985); E. Pahl, H.-D. Meier,

- and L. S. Cederbaum, *Z. Phys. D* **38**, 215 (1996).
- [40] J. Wasilewski, *Int. J. Quantum Chem.* **36**, 503 (1989).
- [41] U. Meier and V. Staemmler, *Theor. Chim. Acta* **76**, 95 (1989).
- [42] J. Wasilewski, *Int. J. Quantum Chem.* **39**, 649 (1991).
- [43] D. E. Woon and T. H. Dunning, *J. Chem. Phys.* **98**, 1358 (1993).
- [44] K. Kaufmann, W. Baumeister, and M. Jungen, *J. Phys. B* **22**, 2223 (1989).
- [45] R. Fink and V. Staemmler, *Theor. Chim. Acta* **87**, 129 (1993).
- [46] K. P. Huber and G. Herzberg, *Molecular Spectra and Molecular Structure IV. Constants of Diatomic Molecules* (Van Nostrand Reinhold, New York, 1979).
- [47] M. N. Piancastelli, M. Neeb, A. Kivimäki, B. Kempgens, H. M. Köppe, K. Maier, A. M. Bradshaw, and R. F. Fink, *J. Phys. B* **30**, 5677 (1997).
- [48] Gy. Víkor, L. Tóth, S. Ricz, Á. Kövér, J. Végh, and B. Sulik, *J. Electron Spectrosc. Relat. Phenom.* **83**, 235 (1997).
- [49] H. M. Köppe, A. L. Kilcoyne, J. Feldhaus, and A. M. Bradshaw, *J. Electron Spectrosc. Relat. Phenom.* **75**, 97 (1995).
- [50] E. J. McGuire, *Phys. Rev. A* **11**, 1880 (1975).
- [51] K. G. Dyall and F. P. Larkins, *J. Phys. B* **15**, 2793 (1982).
- [52] J. Tulkki, T. Åberg, A. Mäntykenttä, and H. Aksela, *Phys. Rev. A* **46**, 1357 (1992).
- [53] J. Tulkki, N. M. Kabachnik, and H. Aksela, *Phys. Rev. A* **48**, 1277 (1993).
- [54] V. Carravetta, H. Ågren, and A. Caesar, *Chem. Phys. Lett.* **148**, 210 (1988).